Reactions of Atomic Hydrogen with Formic Acid and Carbon Monoxide in Solid Parahydrogen I: Anomalous Effect of Temperature

ARTICLE *in* THE JOURNAL OF PHYSICAL CHEMISTRY A · AUGUST 2014

Impact Factor: 2.69 · DOI: 10.1021/jp502470j · Source: PubMed

4 AUTHORS, INCLUDING:

Fred Mutunga
University of Wyoming
3 PUBLICATIONS **5** CITATIONS
SEE PROFILE

Shelby Follett
University of Wyoming
2 PUBLICATIONS **5** CITATIONS
SEE PROFILE

THE JOURNAL OF PHYSICAL CHEMISTRY A

Article

pubs.acs.org/JPCA

Reactions of Atomic Hydrogen with Formic Acid and Carbon Monoxide in Solid Parahydrogen I: Anomalous Effect of Temperature

Leif O. Paulson,† Fredrick M. Mutunga, Shelby E. Follett, and David T. Anderson*

Department of Chemistry, University of Wyoming, Laramie, Wyoming 82071, United States

Supporting Information

ABSTRACT: Low-temperature condensed phase reactions of atomic hydrogen with closed-shell molecules have been studied in rare gas matrices as a way to generate unstable chemical intermediates and to study tunneling-driven chemistry. Although parahydrogen (pH_2) matrix isolation spectroscopy allows these reactions to be studied equally well, little is known about the analogous reactions conducted in a pH_2 matrix host. In this study, we present Fourier transform infrared (FTIR) spectroscopic studies of the 193 nm photoinduced chemistry of formic acid (HCOOH) isolated in a pH_2 matrix over the 1.7 to 4.3 K temperature range. Upon short-term irradiation the HCOOH readily undergoes photolysis to yield CO, CO_2, HOCO, HCO and H atoms. Furthermore, after photolysis at 1.9 K tunneling reactions between migrating H atoms and trapped HCOOH and CO continue to produce HOCO and HCO, respectively. A series of postphotolysis kinetic experiments at 1.9 K with varying photolysis conditions and initial HCOOH concentrations show the growth of HOCO consistently follows single exponential (k = 4.9(7)x10^{-3} min^{-1}) growth kinetics. The HCO growth kinetics is more complex displaying single exponential growth under certain conditions, but also biexponential growth at elevated CO concentrations and longer photolysis exposures. By varying the temperature after photolysis, we show the H atom reaction kinetics qualitatively change at ~2.7 K; the reaction that produces HOCO stops at higher temperatures and is only observed at low temperature. We rationalize these results using a kinetic mechanism that involves formation of an H···HCOOH prereactive complex. This study clearly identifies anomalous temperature effects in the reaction kinetics of H atoms with HCOOH and CO in solid pH_2 that deserve further study and await full quantitative theoretical modeling.

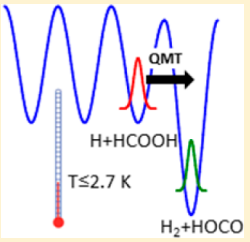

1. INTRODUCTION

Reactions of migrating H atoms with trapped molecular species in frozen parahydrogen (pH_2) crystals provide a relatively unexplored yet well-established experimental method to study the kinetics of condensed phase tunneling reactions in the 1.7 to 4.3 K temperature range. Under these extreme low temperature conditions, almost all exothermic H atom reactions with significant activation energies (e.g., $E_a \geq 2.0$ kcal mol^{-1}) are well below the crossover temperature at which "under the barrier" quantum mechanical atom tunneling dominates over classical "over the barrier" reaction dynamics.[1] This temperature range also corresponds to the energetics of long-range intermolecular forces between the H atom and coreactant, which as we will show in this work, can exert the dominant control mechanism for which reactions proceed. Gas phase studies at temperatures approaching this temperature range repeatedly demonstrate that intermolecular forces in the entrance channel to reaction can dramatically enhance or diminish bimolecular reactivity.[2−4] In solid pH_2, the balance of intermolecular forces between the reactant−reactant, reactant−pH_2, and pH_2−pH_2 within the solid environment can lead to stabilization or destabilization of prereaction complexes of the H atom with a coreactant. Further, the stability of these prereactive complexes can likely be altered by raising the temperature of the sample over the accessible temperature range. H atom reactions with stable molecules in this deep tunneling regime can therefore proceed via nonstandard kinetic mechanisms that are controlled by the stability and average lifetime of the prereactive complex.

The case of H atom reactions in solid pH_2 is especially interesting because H atoms can readily diffuse in solid pH_2 via a mechanism similar to "Grotthuss diffusion" for the motion of protons in liquid water.[5] H atoms in solid pH_2 translate using a "bucket line" mechanism whereby an H atom diffuses through the solid by repeated H + H_2 → H_2 + H tunneling exchange reactions.[6−8] Indeed, the H + H_2 reaction is the prototypical bimolecular reaction in chemical physics, however, its low temperature (below 100 K) behavior was not studied theoretically[9,10] until H atoms were first detected in solid hydrogen at liquid helium temperatures and shown to be mobile 30 years ago.[6,11,12] Much of the subsequent progress in our understanding of H atoms trapped in solid pH_2 has been provided by electron spin resonance (ESR) studies.[13−17] These ESR measurements show that for highly enriched pH_2 samples (i.e., less than 0.1% orthohydrogen (oH_2) concentrations), the H atom recombination rate is too slow to be explained by the diffusion coefficient, which suggests that the H atoms do not recombine efficiently.[16] Further, since the H + H_2 chemical exchange reaction is thermoneutral, the H atom can become delocalized within the pH_2 solid by this resonant tunneling

Received: March 11, 2014
Revised: August 6, 2014

   dx.doi.org/10.1021/jp502470j | J. Phys. Chem. A XXXX, XXX, XXX−XXX

mechanism if the energies of the H atom at different lattice positions within the solid are degenerate.[7,16] Therefore, we expect H atom quantum diffusion in chemically doped pH_2 quantum solids to play an important role in the measured low temperature chemistry.

Fushitani and Momose used Fourier transform infrared (FTIR) spectroscopy[18] to measure the H atom diffusion rate by studying the H + NO → HNO tunneling reaction after the in situ photolysis of NO in solid pH_2 at 5.2 K. In these studies the H atoms are produced as byproducts of the NO photolysis, and the H atom diffusion rate is determined from the growth in the IR absorption intensity of the HNO product. These researchers found H atom diffusion rates 100 times larger than the previous ESR measurements of H atom recombination and ascribed the difference to the intermolecular interactions of H + NO compared to H + H.[18] Andrews and co-workers studied the induced IR transitions in solid hydrogen (and enriched pH_2 solids) produced by the presence of an H atom either by laser ablating metal atoms into the solids or by direct condensation of hydrogen gas subjected to tesla coil discharge in a quartz tube.[19,20] In these studies, H atom-induced peaks in pH_2 were identified at 4151.8 cm^{-1}, which show intensity half-lives compatible with the ESR measurements. More recently, Cao et al. performed 193 nm photolysis studies on HCOOH/HBr mixtures in a Kr matrix aimed at studying the H + HCOOH reaction at low temperature.[21] The experimental protocol in the Kr matrix work involves photolysis at 4.3 K followed by raising the temperature of the sample to 31 K to induce H atom mobility. As we will show, these Kr matrix studies provide interesting comparisons to the present work.

We utilize the 193 nm photochemistry of formic acid (HCOOH) in solid pH_2 to initiate the low temperature chemistry. There are five open photodissociation channels at 193 nm, namely,[22]

$$HCOOH + h\nu \rightarrow HCO + OH \quad (1a)$$

$$\rightarrow HCOO + H \quad (1b)$$

$$\rightarrow H + HOCO \quad (1c)$$

$$\rightarrow CO + H_2O \quad (1d)$$

$$\rightarrow CO_2 + H_2 \quad (1e)$$

where channels 1a−1c represent the radical channels, and channels 1d and 1e are the molecular channels. The gas phase UV photochemistry of HCOOH has been extensively studied,[22−28] and at 193 nm excitation energies there is general agreement that the molecular channels 1d and 1e are significant along with the HCO + OH radical channel (1a). While H atoms can be generated directly via channels 1b and 1c, these two channels are thought to be negligible. We believe the dominant mechanism by which H atoms are generated in solid pH_2 during irradiation is via channel 1a, which produces HCO + OH. The OH can then react with the pH_2 host via the reaction $OH + H_2 \rightarrow H_2O + H$, and we have previously demonstrated indirect evidence of this reaction by detecting transient *para*-H_2O satellite absorption features.[29,30] These satellite features are produced by H_2O that are formed in defect sites following the $OH + H_2$ reaction. Further, HCO can undergo secondary photolysis to produce H + CO, which is another possible source of H atoms.[31] The 193 nm in situ photolysis of HCOOH therefore allows us to trap H atoms, HCOOH, and other photoproducts (e.g., CO, H_2O and CO_2) in solid pH_2 and study the ensuing chemical reactions using FTIR spectroscopy. Under low temperature conditions all the molecules are presumed immobile, but the H atoms can still migrate through the solid via the tunneling exchange mechanism and therefore can potentially react with the various trapped chemical impurities.

In this work we provide experimental evidence for the nonstandard low temperature tunneling kinetics of the H + HCOOH → H_2 + HOCO and H + CO → HCO reactions occurring in solid pH_2 after 193 nm in situ photolysis of HCOOH. By nonstandard we mean that the growth of the HOCO and HCO reaction products only occurs at temperatures below ∼2.7 K, displaying a strong inverse temperature effect. We recently reported[32] on a similar non-Arrhenius behavior for the H + N_2O tunneling reaction in solid pH_2 following the 193 nm photolysis of N_2O. In the present work, we study the H atom reaction kinetics that occur after the 193 nm photolysis of HCOOH under a variety of experimental conditions to develop a qualitative mechanistic model. While the reaction conditions in solid pH_2 are admittedly quite unique compared to other low-temperature molecular ices, we believe many of the lessons learned in this study can find applications in other chemical systems where low-temperature H atom reactions occur. In the accompanying paper[33] (hereafter referred to as Part 2), we provide further tests of our kinetic understanding of this reaction by conducting isotopically substituted (e.g., DCOOD, HCOOD, DCOOH) reaction studies.

2. EXPERIMENTAL SECTION

Our experimental apparatus is described in detail elsewhere;[29,30,34] briefly, we grow millimeters thick, chemically doped pH_2 crystals via rapid vapor deposition[35,36] of independent gas streams of dopant (HCOOH) and pH_2 host onto a BaF_2 optical substrate maintained at approximately 2.5 K inside a liquid helium bath cryostat. The pH_2 host in these studies is enriched to 99.97% pH_2 levels using a variable temperature ortho/para catalytic converter operated near 14.0 K. FTIR spectroscopy is performed on the sample using a normal incidence transmission optical setup. The measured integrated intensities of specific solid pH_2 IR absorptions allow us to determine the IR path length through the sample,[37] which permits the concentration of different species within the crystal to be determined using a Beer's Law expression,

$$[X] = \frac{2.303 \int \log_{10}(I/I_0) d\tilde{\nu}}{\varepsilon(\text{cm mol}^{-1}) d(\text{cm})} (23.16\ \text{cm}^3\ \text{mol}^{-1})(1 \times 10^6) \quad (2)$$

where [X] is the concentration of species X in parts per million (ppm), ε is the gas phase integrated absorption coefficient, d is the IR path length, and V_0 = 23.16 cm^3 mol^{-1} is the molar volume[38] of solid pH_2. The concentrations of the various chemical species studied in this work are determined using eq 2 and the integrated absorption coefficients listed in Table S1 (see Supporting Information (SI)). The accuracy of the reported concentrations likely varies for each molecule studied, but we estimate the error in the concentration of HCOOH to be on the order of ±20% based on the concentrations determined using the ν_1 and ν_2 absorptions.

Photolysis is achieved using the 193 nm output of an ArF excimer laser (Gam Laser EX5) configured to pass through the sample at an angle of 45° with respect to substrate surface normal. This optical setup permits FTIR spectra to be recorded

dx.doi.org/10.1021/jp502470j | J. Phys. Chem. A XXXX, XXX, XXX−XXX

within the photolyzed region of the crystal either during or immediately after 193 nm irradiation. The typical experimental procedure is to photolyze an as-deposited sample at 1.9 K for a short period of time and then take repeated FTIR spectra with short acquisition times (e.g., 3 min for 16 coadded scans at 0.05 cm^{-1} resolution) to measure the low temperature kinetics after photolysis. For most of the kinetic data presented in this work, we use the FTIR configured with a glowbar source, KBr beam splitter, and InSb detector optimized for the 1800 to 5000 cm^{-1} region. However, we also characterize the solid at various times during the experiment using a MCT detector to gain access to the region from 800 to 1800 cm^{-1}.

3. RESULTS

3.1. IR Spectroscopy of Formic Acid and the Photoproducts. We previously characterized the infrared spectroscopy of formic acid (specifically *trans*-HCOOH) trapped in solid pH_2,[34] and here we will use the C−H stretching mode (ν_2) with a peak at 2942.07 cm^{-1} to monitor the formic acid (FA) concentration. We choose the ν_2 absorption feature because it provides a relatively strong but unsaturated absorption peak (using the InSb detector) for the FA concentration range used in these studies. Shown in Figure 1

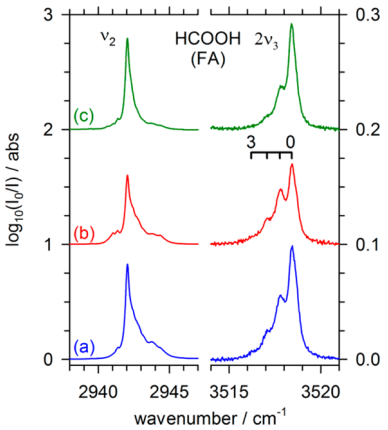

Figure 1. FTIR absorption spectra (spectra are offset vertically for ease of comparison) in the HCOOH (FA) ν_2 and $2\nu_3$ regions for a FA/pH_2 sample showing the effects of 193 nm photolysis and time. Trace (a) is recorded at 1.94 K before photolysis, trace (b) is recorded immediately after 3 min of photolysis (100 μJ cm^{-2} $pulse^{-1}$, 36,000 pulses, 200 Hz), and trace (c) is recorded 425 min after trace (b) while maintaining the sample at 1.94(1) K. All three spectra were recorded at 0.03 cm^{-1} resolution with 6.35 min acquisition times. The absorptions are due to $FA(oH_2)_n$ clusters and the n cluster assignment for the $2\nu_3$ absorption feature is shown by the scale above trace (b). This sample is 0.21(1) cm thick with an initial FA concentration of 65 ppm.

are three spectra in the ν_2 and $2\nu_3$ regions of FA recorded at different times during the course of a 193 nm photochemistry experiment. Trace (a) is recorded at 1.94 K, approximately 35 min after deposition and before photolysis. The ν_2 line shape qualitatively matches the previously reported spectrum;[34] however, the spectrum reported here is for a more concentrated FA/pH_2 sample. Using the ν_2 integrated intensity and measured sample thickness; we estimate that the initial FA concentration is 65(13) ppm. Trace (b) in Figure 1 is recorded with an FTIR acquisition time of 6.35 min beginning immediately after a 3 min duration of 193 nm irradiation (100 μJ cm^{-2} $pulse^{-1}$, 36 000 pulses, 200 Hz) of the sample held at 1.94 K (the temperature rises slightly to 1.96 K during photolysis). As expected, comparison of traces (a) and (b) in Figure 1 shows a diminution in the ν_2 intensity following the in situ photodissociation of FA. Note the ν_2 peak is only reduced by 23% for this amount of 193 nm photolysis, indicating there is still approximately 50(10) ppm of FA in the solid after photolysis. Trace (c) in Figure 1 is the spectrum recorded 425 min after trace (b) while the sample is maintained at 1.94(1) K. It appears that the ν_2 intensity increases between traces (b) and (c); however, this is not the case. The total integrated intensity of the ν_2 peak (integrated from 2938 to 2947 cm^{-1}) stays relatively constant, but the line shape changes such that the peak intensity increases at the expense of absorption intensity in the low and high energy wings.

These slow changes in the FA ν_2 line shape after photolysis are likely caused by molecular hydrogen nuclear spin conversion (NSC). We have previously shown that trace amounts of oH_2 present in the enriched pH_2 solid preferentially cluster to the FA dopant during deposition and upon annealing the sample at 4.3 K.[34,39] The individual $FA(oH_2)_n$ clusters in the size range between n = 0 to n = 5, where n is the number of oH_2 molecules in the cluster, can be spectrally resolved using either the ν_3 or $2\nu_3$ absorption features.[34] For the $2\nu_3$ absorption feature, there is an approximately constant 0.74(9) cm^{-1} shift in the peak maximum of each $FA(oH_2)_n$ cluster to lower wavenumbers with increasing n over this range. This n cluster assignment for the $2\nu_3$ absorption feature is shown by the scale just above trace (b) in Figure 1. For the as-deposited sample before photolysis the $2\nu_3$ absorption feature shows that the dominant peak is the n = 0 peak at 3518.42 cm^{-1}; however, the distribution extends out to n = 3 even for this pH_2 sample with a nominal 300 ppm oH_2 concentration. After photolysis, the entire $2\nu_3$ absorption feature is reduced in intensity, but during the subsequent 7 h reaction time period there is a noticeable increase in the intensity of the n = 0 peak as larger n clusters are converted to smaller clusters via intracluster H_2 NSC. Accordingly, we assign changes in the ν_2 line shape that occur after photolysis to these same NSC effects; however, the individual cluster peaks are not resolved for the ν_2 absorption making it difficult to analyze the line shape changes in detail. As we will show, these line shape changes make quantitative FA concentration measurements problematic using Beer's law spectroscopy.

We can use the same spectra to measure the amount of CO and CO_2 photoproducts that are produced by the 193 nm in situ photolysis of FA. Shown in Figure 2 are the same three spectra shown in Figure 1, only now in the regions of the CO fundamental and CO_2 ν_3 absorption features. We do not observe significant changes in the CO or CO_2 lineshapes after photolysis in contrast to the changes observed for FA. The IR spectra of CO and CO_2 solvated in solid pH_2 have been characterized previously.[40,41] The CO fundamental spectrum is consistent with a nearly free rotating CO localized in a single substitution site and has resolved rovibrational structure.[40] In contrast, the CO_2 spectrum is indicative of a nonrotating CO_2 that occupies a double substitution site and there are several extremely sharp absorption peaks in the ν_3 region.[41] Trace (a) in Figure 2, recorded before photolysis, only shows weak CO_2 peaks due to CO_2 molecules deposited in the pH_2 sample from the cryostat thermal isolation vacuum gas.[35,36] While CO_2 is present in the pH_2 solid prior to photolysis, the concentration is much less than 1 ppm (e.g., ~0.04 ppm). After photolysis, both CO and CO_2 are present at significant levels as expected

dx.doi.org/10.1021/jp502470j | J. Phys. Chem. A XXXX, XXX, XXX−XXX

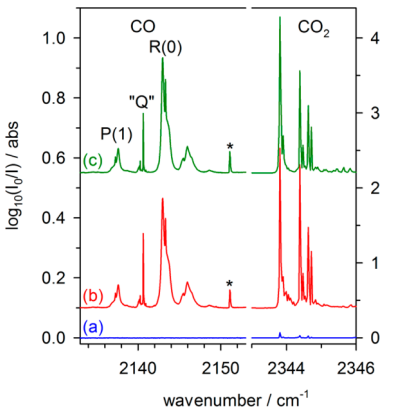

Figure 2. FTIR spectra in the regions of the CO fundamental and CO_2 ν_3 mode for the same spectra described in Figure 1, showing CO and CO_2 are produced by photolysis. The peak marked with an asterisk is assigned to the CO−H_2O complex. Spectra are offset vertically for ease of comparison.

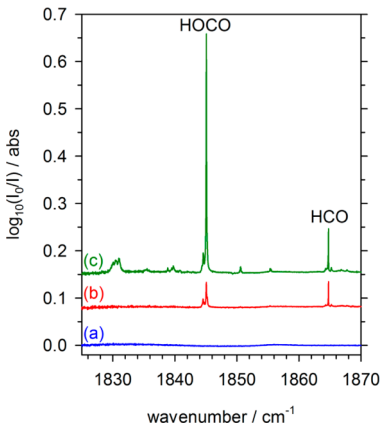

Figure 3. FTIR spectra from 1825 to 1870 cm^{-1} for the same spectra described in Figure 1 displaying continued growth of HOCO and HCO after photolysis. The additional unlabeled peaks in this region are likely due to HOCO or HCO clustered with another species. Spectra are offset vertically for ease of comparison.

for photoproduction via molecular channels 1d and 1e, respectively. Based on the spectral measurements for six separate FA-doped pH_2 photolysis experiments, we estimate that the CO/CO_2 branching ratio is 8.7(12), where the error in parentheses is the 2σ standard deviation for the six measurements. In the gas phase, the CO/CO_2 branching ratio was measured[22] to be 11, which is qualitatively reproduced by theory.[27,28] This indicates that the FA photodissociation dynamics are only weakly perturbed by the presence of the pH_2 solid. Furthermore, these molecular photoproducts are produced as well-isolated monomers unlike similar 193 nm photolysis studies of FA in Ar or Xe matrices where CO−H_2O and CO_2−H_2 van der Waals complexes are formed almost exclusively.[42−44] The rare gas matrix results are typical of matrix isolation photochemistry where the matrix cage around the photoactive molecule keeps the photofragments in close proximity and prevents them from escaping the matrix cage.[44] As demonstrated in many other pH_2 matrix photolysis studies, the in situ photoproduction of isolated CO and CO_2 monomers indicates the photodynamics is anomalous due to the lack of a significant cage effect in solid pH_2.[45,46] However, we do detect CO−H_2O clusters; the cluster peak is marked with an asterisk in Figure 2. We assign this cluster peak by performing double doping control experiments (see Figure S1 in the SI). We also detect CO−FA clusters after photolysis, which again suggests that the photofragments easily escape the solvent cage. The small amount of CO−FA cluster formation measured after photolysis likely proceeds via long-range ballistic migration of the photofragments resulting in collisions with other dopant species and cluster formation.

The radical photoproducts HOCO and HCO are also produced in the 193 nm in situ photochemistry of FA; however, the majority of radical photoproducts are generated well after photolysis is stopped via subsequent H atom reactions. Shown in Figure 3 are spectra from 1825 to 1870 cm^{-1} for the same FA/pH_2 photochemical experiment described in Figure 1. This spectral region should contain peaks due to the strong carbonyl stretching modes of both *trans*-HOCO (hereafter referred to as HOCO) and HCO. We presented IR spectra of all three modes of HCO in previous studies of the 193 nm in situ photolysis of *N*-methylformamide in solid pH_2.[47] We show in Figure S2 in the SI detailed lineshapes of the ν_2 (CO stretch) and ν_1 (CH stretch) fundamentals of HCO at 1.65 and 4.36 K, which show better resolved spectra than previously reported.[47] We suspect the fine structure observed in both bands is due to hindered rotation and/or spin-rotation interactions. This is the first report of HOCO in solid pH_2, and accordingly we present all the observed spectral features in Table S2 and Figure S3; representative HOCO ν_1 and ν_2 IR spectra at low and high temperature are provided in Figure S4 (see SI). For HOCO we only observe fine structure (additional peaks to the red of the main peak) in the low temperature scans ($T \leq 1.8$ K). Unlike HCO, we do not expect hindered rotation (except possibly K-rotation) for HOCO, and the spin-rotation interaction is too small to produce measurable splittings. We determine the HOCO concentration using the average measured from the ν_1 and ν_2 absorptions.

As shown in trace (a) of Figure 3, there are no detectable peaks due to either HOCO or HCO before photolysis. In trace (b), the first FTIR spectrum recorded immediately after photolysis, absorption features due to HOCO and HCO are detected; however, both of these absorptions (especially the HOCO peak) only increase significantly well after photolysis while the sample is maintained at 1.94(1) K, as shown in trace (c) of Figure 3 recorded 425 min after trace (b). As we will show, these HOCO and HCO peaks increase due to dark reactions of H atoms with unphotolyzed FA and the photogenerated CO, respectively. The other unlabeled small absorptions shown in trace (c) of Figure 3 are likely due to HOCO and HCO clustered to H_2O or FA; however a detailed assignment was not conducted. We have shown previously that photodissociation of FA produces transient para-H_2O satellite peaks which we believe are produced by photodissociation along channel 1a followed by reaction of the OH with the pH_2 matrix ($OH+H_2 \rightarrow H_2O+H$) to form *para*-$H_2O$ and H atoms;[29,30] this is likely the dominant pathway by which H atoms are produced. While HOCO and HCO are also generated directly via the in situ UV photochemistry of FA (channels 1a and 1c), efficient secondary photolysis of the radical photoproducts occurs during irradiation thereby limiting the amount of radical photoproducts that can be produced by photolysis alone.

3.2. Postphotolysis H Atom Reaction Kinetics. To investigate the mechanism of the low-temperature reactions

dx.doi.org/10.1021/jp502470j | J. Phys. Chem. A XXXX, XXX, XXX−XXX

leading to the production of HOCO and HCO, we performed a number of experiments on FA-doped pH_2 samples. First we characterize the as-deposited sample using FTIR spectroscopy, then irradiate the sample with 193 nm radiation for a short period of time, and finally record a set of repeated rapid scan FTIR spectra to measure the kinetics of the postphotolysis dark reactions. For example, the full kinetic data acquired for the experiment discussed so far is displayed in Figure 4. The arrows

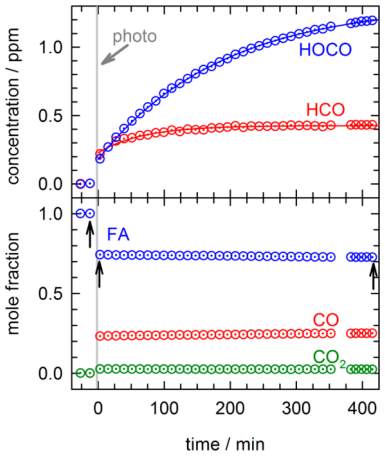

Figure 4. Kinetic plots of concentration versus time recorded before and after photolysis for the FA/pH_2 sample depicted in Figure 1. The photolysis interval is indicated by a gray vertical bar. The data are represented by dotted circles and the lines are the result of least-squares fits of the data to eq 3 (see text for details). The arrows indicate which rapid scan FTIR spectra are shown in traces (a), (b), and (c) in Figures 1−3.

in Figure 4 indicate which data points correspond to the FTIR spectra displayed in Figures 1−3 for this experiment. The gray vertical bar represents the time and duration of the 193 nm photolysis exposure. In order to show the relative concentrations of FA, CO, and CO_2 before and after photolysis, we convert the measured concentrations (in ppm) to mole fractions by dividing the concentration of one of the species by the sum of all three. As shown in Figure 4, before photolysis, the sample contains FA at a mole fraction close to 1.0 and negligible concentrations of CO and CO_2. After photolysis, the mole fraction of FA drops to 0.74, and the CO and CO_2 concentrations increase to 0.23 and 0.03, respectively. After photolysis, the concentrations of FA, CO, and CO_2 remain relatively constant and along with H_2O (not shown) constitute the most concentrated chemical species in the pH_2 matrix. However, the concentrations of HOCO and HCO continue to increase starting from around 0.18 and 0.22 ppm right after photolysis, and increasing to 1.2 and 0.43 ppm, respectively.

At these low temperatures (T = 1.94 K) we assume that all the chemical impurities mentioned above are immobilized except for the H atoms, and thus we suspect bimolecular H atom reactions with other species in the matrix lead to the formation of HOCO and HCO. In one of the first FA photochemistry experiments, we checked for the possibility of IR driven reaction dynamics (caused by the IR light of the FTIR spectrometer) similar to the type observed for atomic chlorine[48] in solid pH_2 by making measurements with a low pass optical filter in the FTIR beam (<3816 cm^{-1}). We still observe growth in HOCO and HCO after photolysis; thus the FTIR beam is not making significant contributions to the observed reaction kinetics. As a first-cut in the kinetic analysis of the data, we least-squares fit the data to a simple first-order growth expression,

$$\Delta C(t) = C_0 + C_1(1 - \exp(-k_1 t)) \quad (3)$$

where C_0 and $C_0 + C_1$ are the concentrations at time zero and infinite reaction time, respectively, and k_1 is the fitted first-order rate constant. Here we define time zero as when the photolysis laser is shut off. The resulting fits to the HOCO and HCO data are shown as solid lines in Figure 4. The fitted parameters are presented in Table S3 and S4, labeled experiment 5, in the SI. The photolysis conditions (duration and repetition rate) and FA concentration after photolysis are also indicated in Table S3. These results clearly show the different kinetic behaviors for the growth of HOCO and HCO. The fitted HCO rate constant (k_1 = 14.7(8) × 10^{-3} min^{-1}) is 2.7 times faster than the HOCO rate constant (k_1 = 5.39(5) × 10^{-3} min^{-1}), but the growth in the HOCO concentration after photolysis is 5.7 times greater than HCO. Note the HCO growth is essentially complete after 150 min, whereas the HOCO concentration continues to grow over the full 425 min duration of the experiment. Given our hypothesis that reactions of H atoms with FA are leading to the growth in HOCO, we therefore expected to observe an exponential decrease in the FA concentration over the same time interval. However, a blow-up of the measured FA concentration with time reveals a nearly linear decrease (~4.9 ppm) over the course of the experiment.

We can better follow the FA concentration changes after photolysis using the $2\nu_3$ absorption feature because we partially resolve the individual $FA(oH_2)_n$ cluster peaks. To extract the n-specific cluster concentrations, we fit the measured $2\nu_3$ absorption feature to a sum of Lorentzian peaks to deconvolute the integrated intensities of each cluster peak; as we showed previously[34] the measured $2\nu_3$ line shape is well modeled by a sum of Lorentzian peaks. We then convert the integrated intensities to concentrations using the $2\nu_3$ integrated absorption coefficient reported in Table S1. Representative fits to the $2\nu_3$ spectra are shown in Figure S5 in the SI. The results of this analysis are plotted in Figure 5 for the same experiment depicted in Figure 4. Photolysis results in the largest decrease in the n = 0 concentration, while changes in the other $FA(oH_2)_n$ cluster concentrations are smaller. Interestingly, both the n = 0 and n = 1 cluster concentrations show fast and slow components in their response to the 193 nm photolysis. In addition, after photolysis the n = 1 concentration continues to decrease, and the n = 0 concentration increases. Presumably, this results from intracluster H_2 NSC. We fit the n = 0 and n = 1 cluster data to biexponential expressions for growth and decay,

$$\Delta C(t) = C_0 + C_1(1 - \exp(-k_1 t)) + C_2(1 - \exp(-k_2 t)) \quad (4)$$

$$\Delta C(t) = C_0 + C_1 \exp(-k_1 t) + C_2 \exp(-k_2 t) \quad (5)$$

and the fitted parameters are reported in Table S5. Both clusters have fast (52(9) × 10^{-3} min^{-1} and 40(10) × 10^{-3} min^{-1}) and slow (5(1) × 10^{-3} min^{-1} and 2(2) × 10^{-3} min^{-1}) rate constants associated with the observed kinetics and the slow rate constant is comparable to the previously reported[34] intracluster $FA(oH_2)_n$ NSC rate constant (k = 2.5(5) × 10^{-3} min^{-1}). However, this slow rate constant is also similar in magnitude to the rate constant extracted from the HOCO growth and therefore changes in the various $FA(oH_2)_n$ cluster

dx.doi.org/10.1021/jp502470j | J. Phys. Chem. A XXXX, XXX, XXX−XXX

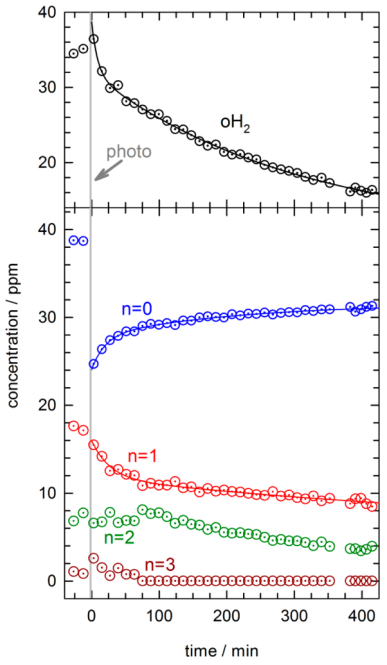

Figure 5. Kinetic plots of the $FA(oH_2)_n$ (n = 0–3) and oH_2 concentrations determined from modeling the FA $2\nu_3$ absorption feature with a sum of Lorentzian lineshapes for the FA/pH_2 sample depicted in Figure 4. The data are represented by dotted circles and the lines are the result of least-squares fits of the data to eq 4 and 5 (see text for details).

concentrations caused by NSC could be masking small changes due to reaction. To assess if the expected FA decay due to reaction with H atoms could be concealed in the data, we quantitatively compare the changes in the n = 0 and n = 1 cluster concentrations determined from the fits. There is a net 2(5) ppm decrease in the FA concentration between the n = 1 and n = 0 clusters associated with the slow rate constant. This suggests that some of the decay in the n = 1 cluster concentration (or lack of growth in the n = 0 cluster) could be due to reactions with H atoms, but because the rate constants for NSC and reaction are comparable, it is impossible to isolate the contributions due to reaction. The kinetic data in Figure 5 also show why we observe an apparent linear decrease in the FA concentration using the ν_2 absorption. The opposing changes in the n = 0 and n = 1 cluster concentrations cancel out when monitored via the ν_2 absorption because the individual cluster peaks are not resolved, and rather only the net change in the total $FA(oH_2)_n$ concentration is observed. For this reason the FA kinetic trace in Figure 4 cannot be interpreted at the quantitative level necessary to detect 1–2% changes in the FA concentration due to reaction. However, as we will show in Part 2 of this series, by using isotopic substitution we can unambiguously prove that the growth in the HOCO concentration shown in Figure 4 is due to H atom reactions with FA. We also note the decay in the total oH_2 concentration determined from the concentration of the $FA(oH_2)_n$ clusters similarly shows fast and slow components to the NSC kinetics (shown in Figure 5). The slow rate constant $(2.1(7) \times 10^{-3}$ $min^{-1})$ extracted from the fit to the oH_2 data is within experimental uncertainty equal to the rate constant $(2.5(5) \times 10^{-3}$ $min^{-1})$ reported previously for intracluster NSC in the absence of H atoms.[34]

To explore the qualitative differences in the growth kinetics of HOCO and HCO further, we performed additional low temperature FA photolysis experiments under varying conditions. The kinetic results of all 6 experiments are presented in Tables S3 and S4; here we describe in detail the results of just one other experiment (expt. 6 in Table S3 and S4). Shown in Figure 6 is a photolysis experiment where we photolyzed the

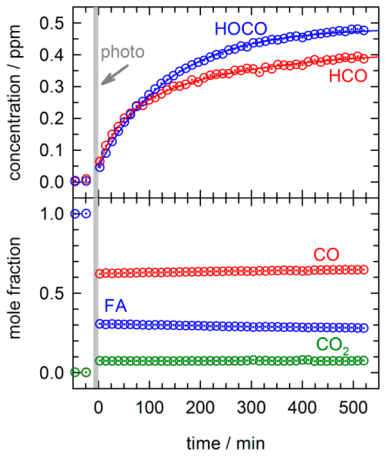

Figure 6. Kinetic plots of concentration versus time recorded before and after photolysis for a FA/pH_2 sample that is 0.20(1) cm thick with an initial FA concentration of 29 ppm. The photolysis interval, indicated by a gray vertical bar, consisted of 576 s of 193 nm irradiation (128 μJ cm^{-2} $pulse^{-1}$, 144 000 pulses, 250 Hz). The data are represented by dotted circles, and the lines are the result of least-squares fits to the data (see text for details).

sample for a much longer period of time (128 μJ cm^{-2} $pulse^{-1}$, 144 000 pulses, 250 Hz) than the experiment depicted in Figure 4. In this case, the FA mole fraction after photolysis has dropped to 0.31, which is less than the 0.62 CO mole fraction. We again fit the growth curves of HOCO and HCO to eq 3 and find the fitted rate constant for HOCO growth $(7.22(10) \times 10^{-3}$ $min^{-1})$ is comparable to the rate constant $(5.39(5) \times 10^{-3}$ $min^{-1})$ determined in the experiment presented in Figure 4. However, in this case, the HCO data did not fit well to a single-exponential expression, but rather is better represented by eq 4 with both slow and fast components (results are presented in Table S4). The fast component ($k_1 = 22(4) \times 10^{-3}$ min^{-1}) has a rate constant comparable to the rate constant extracted from the data shown in Figure 4 for HCO, however now there is also a slow component ($k_2 = 3.9(9) \times 10^{-3}$ min^{-1}) to the HCO growth. This slower rate constant is similar in magnitude to the one extracted for HOCO. The magnitude of this slow process in the HCO growth is more significant under these conditions of greater CO mole fraction and photolysis time compared to the kinetic data in Figure 4. We will examine these differences in more detail in the Discussion section.

3.3. Reaction Temperature Dependence. After we conducted the six low temperature ($T \approx 1.9$ K) FA photolysis experiments presented in this work, we decided to see if the reaction kinetics changed at higher temperatures. The first high temperature experiment (T = 4.3 K) was performed using a deuterated FA sample (DCOOD) and these results are presented in Part 2. To our surprise, we observed no evidence for postphotolysis reactions when the sample temperature was rapidly increased to 4.3 K right after photolysis at 1.9 K. We expected the H atom diffusion rate to be approximately

dx.doi.org/10.1021/jp502470j | J. Phys. Chem. A XXXX, XXX, XXX–XXX

constant[16] over this small temperature range, and therefore the reaction should readily occur at the higher 4.3 K temperature. Based on these preliminary "high-temperature" results for the lack of postphotolysis reactions, we decided to return to the FA/pH_2 system to measure how the reaction kinetics change as a function of temperature over the 1.7 and 4.4 K range. To accomplish this, we photolyze the FA/pH_2 sample at 4.34(1) K and then slowly lower the temperature to determine at what temperature the kinetics qualitatively change and the reaction starts to occur. The results of this experiment are shown in Figure 7. We deposit a FA/pH_2 sample at 2.5 K with an FA

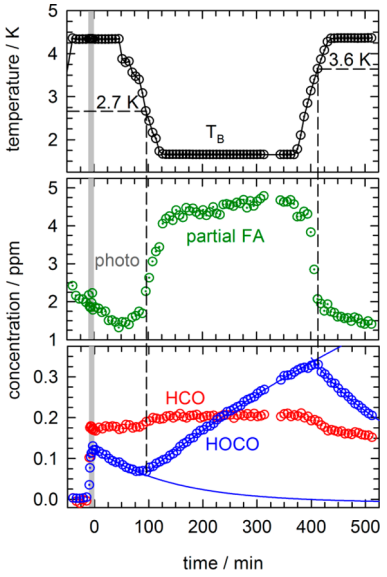

Figure 7. Kinetic plot for a photolysis (70 μJ cm^{-2} pulse^{-1}, 150 000 pulses, 250 Hz) and reaction study conducted on a FA/pH_2 sample as a function of temperature. The top graph shows the temperature measured at the beginning of each FTIR scan, the middle graph shows the partial FA concentration (see text for details), and the bottom graph shows the measured HOCO (blue circles) and HCO (red circles) concentrations. The lines in the bottom graph are the results of least-squares fits to the data. This experiment shows that for a sample photolyzed at 4.33 K, the reaction that produces HOCO after photolysis only starts the first time the temperature is lowered below ~2.7 K. The kinetics of this reaction again qualitatively changes at later times when the temperature is raised above 3.6 K. Note only the HOCO kinetics show the abrupt changes with temperature.

concentration of around 43(9) ppm. We raise the temperature to 4.34(1) K and record four repeated FTIR spectra to characterize the sample before photolysis. The sample is then irradiated (106 μJ cm^{-2} pulse^{-1}, 250 Hz, 10 min) with the 193 nm laser radiation at 4.34(1) K. We maintain the sample temperature at 4.34(1) K for approximately 50 min after photolysis and then start to cool the sample. For these first 50 min the HOCO and HCO concentrations behave as in other high-temperature kinetic experiments; the HOCO concentration steadily decays, while the HCO concentration remains constant. We can fit the HOCO data for these first 50 min at 4.34(1) K to a simple three-parameter exponential decay expression, and the results of the fit are plotted in Figure 7 as a blue line. We extract $k = 7.1(29) \times 10^{-3}$ min^{-1} from the initial HOCO decay. At approximately the 96 min mark, at a temperature of 2.7 K, the HOCO kinetics change qualitatively and switch from steadily decreasing to increasing. This transition occurs abruptly at ~2.7 K as determined by the starting temperature measured for the first FTIR scan where the HOCO concentration increases. We continue to maintain the temperature at the low value of 1.65(1) K from approximately 125 to 375 min after photolysis. During this time the HOCO concentration steadily increases, and the HCO concentration remains constant. The slight increase in the HCO concentration as the temperature is lowered is due to physical changes in the HCO solvation environment and not thought to reflect irreversible concentration changes. If we fit the HOCO data to eq 3 over the entire period where the temperature is maintained below 2.7 K, we determine a HOCO growth constant of $k = 1.15(13) \times 10^{-3}$ min^{-1}, which is comparable to the average rate constant ($k = 4.9(17) \times 10^{-3}$ min^{-1}) measured for the six separate low temperature experiments. Thus, it appears the reaction kinetics is similar except the reaction only starts at temperatures below ~2.7 K. Finally, at around the 375 min mark we again increase the temperature of the sample to 4.35(1) K. As can be seem in Figure 7, as the temperature increases to above 3.6 K the HOCO kinetics again qualitatively change from steadily increasing to decreasing ($k = 5.8(12) \times 10^{-3}$ min^{-1}). This change in the kinetics occurs at a higher temperature than when we originally cooled the sample from 4.34(1) K. In contrast, the HCO concentration decreases slightly back to the original value measured at 4.34(1) K right after photolysis. It is important to point out the FA concentration after photolysis for the sample shown in Figure 7 was roughly 35 ppm, and the CO concentration was 4.0 ppm; under these conditions we expect only a minor amount of reaction of the H atoms with CO compared to FA.

To try to understand what is physically changing within the pH_2 solid over this small temperature range to account for the different kinetic behaviors, we include in Figure 7 the partial FA concentration (partial FA). As we show in Figure S6 in the SI, if instead of integrating the entire FA ν_2 peak we only integrate the low energy wing of the absorption, we can convert this partial integrated intensity into a partial FA concentration using the ν_2 absorption coefficient. The ν_2 line shape changes with temperature such that the intensity of a shoulder peak increases at low temperature (see Figure S6). As shown in Figure 7, the converted partial FA concentration therefore reversibly cycles between low values at high temperature and high values at low temperature. These temperature dependent changes in the FA ν_2 line shape are reversible and signal physical changes in the immediate FA solvation environment. We only observe these reversible changes in the ν_2 line shape with temperature, not the $2\nu_3$ absorption. We speculate these changes in the FA solvation environment as measured using the ν_2 absorption are somehow related to the observed qualitative change in the reaction kinetics.

To test the reproducibility of these temperature effects on the reaction kinetics we conducted another experiment on a different FA/pH_2 sample, where instead we photolyzed the sample at low temperature and then raised the temperature approximately 2 h after photolysis. The results of this experiment are shown in Figure 8. This sample contained 39(8) ppm of FA after photolysis and 5.4 ppm of CO. Again we observe a qualitative change in the HOCO growth kinetics when the temperature is raised from 1.82(1) K to above ~3.6 K. Similar to the results shown in Figure 7, when the sample temperature is increased at first the HOCO concentration levels off and then starts to decrease making it harder to precisely determine at what temperature the change in the

dx.doi.org/10.1021/jp502470j | J. Phys. Chem. A XXXX, XXX, XXX−XXX

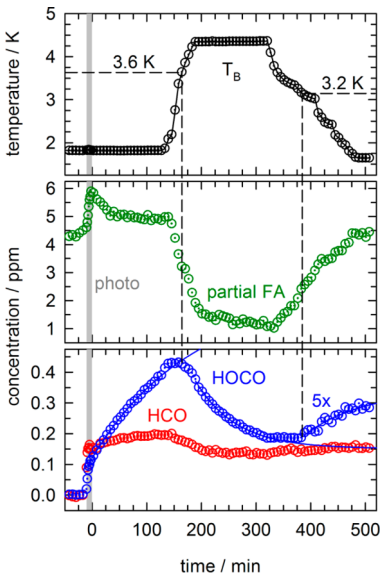

Figure 8. Kinetic plot for the photolysis (48 μJ cm^{-2} pulse^{-1}, 150 000 pulses, 250 Hz) and reaction study conducted on a FA/pH_2 sample as a function of temperature. The top graph shows temperature, the middle graph the partial FA concentration (see text for details), and the bottom graph the measured HOCO (blue circles) and HCO (red circles) concentrations. The lines in the bottom graph are the results of least-squares fits to the data. Note the concentration differences have been multiplied by 5 beginning at the ~375 min mark to show the kinetics after the temperature is lowered below 3.2 K for the second time.

kinetics occurs. If we fit the HOCO data for approximately the first 120 min when the sample temperature is maintained at 1.81(1) K, we get a fitted rate constant of $k = 5.5(4) \times 10^{-3}$ min^{-1}, which compares favorably with the average low temperature rate constant ($k = 4.9(17) \times 10^{-3}$ min^{-1}). While the sample temperature is held at 4.34(1) K the HOCO concentration steadily decays with single exponential kinetics. At approximately the 325 min mark after photolysis, we begin to gradually lower the temperature again. Even 380 min after the photolysis is stopped, once the temperature is lowered below ~3.2 K the HOCO growth starts to occur again albeit with a decreased magnitude. To better show the increase in the HOCO concentration at this point in the experiment, we multiplied the concentration difference by a factor of 5 in Figure 8. If we fit the data to eq 3, we get a fitted rate constant of $k = 9.3(43) \times 10^{-3}$ min^{-1}. The partial FA concentration behaves as it did in the first variable temperature experiment. However, in this case it also shows a fast kinetic response right after photolysis at low temperature. This behavior is observed in other low temperature photolysis experiments as well; the partial FA concentration rapidly increases during photolysis and then rapidly decays right after photolysis is stopped. Note also that in contrast to the changes in the HOCO concentration, the HCO concentration stays relatively constant after photolysis over the entire course of the experiment due presumably to the lack of H atom reactions with CO at these low CO concentrations.

4. DISCUSSION

The tunneling reactions H + FA and H + CO are both necessarily exothermic, otherwise these reactions could not occur even by a tunneling mechanism at these low temperatures, but both are expected to have significant reaction barriers. The H + FA reaction is predicted to proceed via an H atom abstraction mechanism to form HOCO and H_2 with roughly a 2840 cm^{-1} barrier[49] and an exothermicity[50] of ΔH = −2560 cm^{-1}. The transition state is predicted to be a linear H−H−C arrangement, where the H atom abstracts from the alkyl C−H bond. The C−H bond must stretch from 1.089 to 1.349 Å to reach the transition state.[49] We do not believe the H atom will abstract the hydroxyl H atom to form the formate radical (HCOO) as oxygen radicals are inherently less stable than carbon radicals, and therefore this reaction channel is likely closed (endothermic) for low-temperature tunneling reactions.[51] More recent ab initio calculations by Cao et al. and Marshall and Glarborg identified an H atom addition channel to initially form *trans*-H_2COOH which can then isomerize to form the more stable *trans*−*cis*-HC(OH)$_2$ conformer.[21,52] These two adducts were identified in the H + FA reaction carried out at 31 K in a Kr matrix following the 193 nm photolysis of a FA/HBr mixture, however, no evidence of these species is provided in this work. The fact that qualitatively different reaction products are observed for the H + FA reaction in a Kr matrix[21] and in solid pH_2 provides further evidence that the reaction mechanisms are likely very different in the two matrices under different experimental conditions. There is a barrier for the H + CO reaction as well: the experimentally determined[53] barrier is low (700 cm^{-1}) and the reaction is more strongly exothermic (ΔH = −5020 cm^{-1}) as estimated from the H−CO bond dissociation energy.[54]

4.1. Limiting Kinetic Behavior. One important question is what does the measured rate constant at low temperature reflect physically? To organize the discussion of this question, and to be consistent with previous researchers,[16,18] we use the kinetic equations developed for reactions in solution.[55,56] For the H + FA and H + CO reactions in solid pH_2 we therefore have

$$\mathrm{H} + \mathrm{FA} \underset{k_{-1}}{\overset{k_1}{\rightleftarrows}} \mathrm{H{-}FA} \xrightarrow{k_2} \mathrm{H_2} + \mathrm{HOCO} \tag{6}$$

$$\mathrm{H} + \mathrm{CO} \underset{k_{-3}}{\overset{k_3}{\rightleftarrows}} \mathrm{H{-}CO} \xrightarrow{k_4} \mathrm{HCO} \tag{7}$$

where k_1 and k_3 are the diffusion-limited rate constants, k_{-1} and k_{-3} are the unimolecular rate constants for dissociation of the encounter complexes (H−FA and H−CO), and k_2 and k_4 are the rate constants for the irreversible tunneling reactions that lead to products. A steady-state treatment for the encounter complex (e.g., H−FA) yields the rate law,

$$\frac{\mathrm{d[HOCO]}}{\mathrm{d}t} = \frac{k_2 k_1}{k_{-1} + k_2}[\mathrm{H}][\mathrm{FA}] \tag{8}$$

Given this rate law, there are two limiting cases typically considered. As postulated previously[16,18] for the H + H → H_2 and H + NO → HNO reactions in solid pH_2, if $k_2 \gg k_{-1}$, then the rate law simplifies to Rate = k_1[H][FA], and the kinetics are said to be "diffusion limited." The other limiting case is called the "slow reaction" limit, where $k_{-1} \gg k_2$, and now the first step is in equilibrium and $k = Kk_2$, where $K = k_1/k_{-1}$. Under these limiting conditions, the rate law simplifies to Rate = k_2[H−FA].

First consider the case where the kinetics is in the slow reaction limit and the extracted rate constant directly reflects the tunneling reaction step. Much of the data presented in this work is qualitatively consistent with this limiting case; fast

dx.doi.org/10.1021/jp502470j | J. Phys. Chem. A XXXX, XXX, XXX−XXX

equilibration between the H atom reagents and the encounter complexes after photolysis followed by a slow tunneling reaction step. First, in none of the experiments did we detect any initial induction period in the growth of either HOCO or HCO, which would be expected for diffusion limited bimolecular reactions that can be initiated rapidly. Second, analysis of the oH_2 concentration using the intensities of the $FA(oH_2)_n$ cluster peaks show the oH_2 concentration decreases very rapidly after photolysis and then more slowly at longer times. This could be caused by mobile H atoms right after photolysis that induce fast NSC catalyzed by the free electron on the H atom, and then slower NSC as the H atoms become trapped next to dopant species. Third, for slow reaction kinetics the bimolecular reaction is transformed into a unimolecular process with the rate determined by the tunneling reaction step (Rate = k_2[H−FA]) and only the amount of HOCO products depends on the initial FA concentration, not the rate. This is consistent with the six low-temperature experiments that measure a rate constant that does not change with the initial FA concentration. If we assume the equilibrium constant K for H−FA is comparable to that for H−CO, then the amount of products detected depends on the relative amounts of FA and CO after photolysis. However, if the H−FA encounter complex has a larger K compared to H−CO, then the products will be skewed toward the production of HOCO. This is demonstrated for the data in Figure 6, which has more CO than FA after photolysis, and yet slightly more HOCO is produced than HCO. Finally, slow reaction kinetics would imply the free H atom concentration is very small, and $K > 1$ equilibrium constants favor the H atoms trapped in encounter complexes. Very quickly after photolysis is stopped, the free H atoms equilibrate with H atoms in the encounter complexes, and this is consistent with our lack of observation of H atom induced IR absorption peaks.[17,18]

Next consider the case where the kinetics is assumed to be diffusion limited. This implies the kinetics should follow a second-order rate law where the extracted rate constant reflects the H atom quantum diffusion coefficient. Given our experimental conditions, it is safe to assume the H atoms are the limiting reagent, and therefore we expect to measure pseudo first-order kinetics (Rate = k_2'[H] where $k_2' = k_2$[FA]) and k_2' should scale linearly with the FA concentration after photolysis. Shown in Figure 9(a) is a plot of the measured HOCO rate constant as a function of the FA concentration after photolysis. Clearly, the extracted rate constant does not scale linearly with the FA concentration. As we will show in Part 2 of this series, the reaction that produces HOCO is unambiguously identified with FA, and thus this discrepancy is not caused by a reaction mechanism that does not involve FA. The data shown in Figure 9(a) is the single most compelling piece of evidence the reaction kinetics are in the slow reaction limit where the extracted rate constant would not scale linearly with the FA concentration. However, we still believe the kinetics are diffusion limited and differences in the details of H atom quantum diffusion compared to classical diffusion cause the deviations from the expected pseudo first-order behavior.[15,16] For example, plotted in Figure 9(b) is the extracted rate constant versus the change in the FA concentration caused by the 193 nm irradiation, and we observe a stronger correlation. Possibly defects or vacancies created by the 193 nm photolysis increase the H atom diffusion rate and mask the linear correlation with the FA concentration.

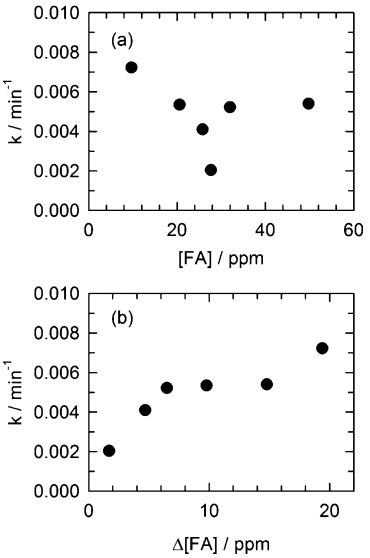

Figure 9. Graphs of the fitted HOCO rate constant using eq 3 versus (a) the FA concentration after photolysis and (b) the change in FA concentration produced by photolysis. Graph (a) shows the data is not consistent with pseudo first-order kinetics with respect to the FA concentration (see text for details).

The answer to the question originally posed at the beginning of this section is that based on the measured HOCO and HCO growth kinetics alone, without detecting the kinetics of one of the reactants or intermediates, we cannot distinguish between diffusion limited or slow reaction kinetics. Either limiting kinetic mechanisms are capable of reproducing the observed kinetic data. The lack of a clear dependence of the measured HOCO rate constant on the FA concentration after photolysis does suggest the reaction kinetics are in the slow reaction limit. However, an important piece of evidence presented in Part 2 indicates the kinetics is in the diffusion limited regime; specifically the lack of a significant kinetic isotope effect for the analogous H atom reactions with fully deuterated FA (DCOOD). Given the tunneling reaction step involves abstraction of an H atom or D atom attached to the carbon atom, one would expect the measured rate constant for H + DCOOD to be significantly smaller if the reaction kinetics is in the slow reaction limit where the rate-determining step is the tunneling reaction. Therefore, even though the reaction kinetics do not show pseudo first-order behavior with respect to the FA concentration, we speculate the kinetics are diffusion limited and the extracted rate constant reflects the diffusion limited rate constant for formation of the H−FA and H−CO encounter complexes.

4.2. Effect of Temperature on the Observed Kinetics.

The most intriguing observation of the present study is the temperature dependence of the H + FA reaction shown in Figures 7 and 8. The likely reason this kinetic behavior has not been reported previously is simply that this combination of low temperature and low oH_2 concentration has not been studied. For example, the H + NO reaction[18] study was conducted for highly enriched pH_2 solids, but only at a single temperature of 5.2 K. Further, the H + NO reaction is an example of a barrierless radical−radical reaction and therefore likely will not show the same temperature dependence as the H + FA reaction which has a significant barrier.

Obviously, characterizing the kinetic mechanism is essential before this anomalous temperature effect can be understood.

dx.doi.org/10.1021/jp502470j | J. Phys. Chem. A XXXX, XXX, XXX−XXX

Based on the discussion in the previous section, if we assume the reaction kinetics is diffusion limited, we can learn by analogy from similar anomalous temperature effects measured for gas phase reactions. For example, recent low temperature gas phase kinetic measurements[3] on the OH + CH_3OH reaction using the CRESU technique show the rate constant at 63 K is approximately 2 orders of magnitude greater than the rate constant at 200 K. These observations prompted the suggestion that "a mechanism involving a weakly bound complex may lead to rate coefficients at low temperatures that are similar in magnitude to those expected for entirely barrierless reaction," and have been interpreted in terms of a reaction mechanism that involves a hydrogen-bonded complex ($E_{H\text{-bond}}$ = −1700 cm^{-1} binding energy) between the OH and CH_3OH reagents in the entrance channel to reaction.[3] The proposed kinetic mechanism is strikingly similar to the mechanism used for reactions in solution,

$$OH + CH_3OH \underset{k_{uni}}{\overset{k_D}{\rightleftarrows}} OH{-}CH_3OH \xrightarrow{k_{rxn}} H_2O + CH_3O \quad (9)$$

where there is a significant reaction barrier (2950 cm^{-1}) between the hydrogen-bonded (H-bonded) complex and the reaction products. Therefore, at high temperature ($T \gg 200$ K) the H-bonded complex rapidly dissociates after formation and the reaction displays normal Arrhenius behavior. However, as the temperature is lowered, the H-bonded complex will be formed on average with less and less internal energy and its lifetime with respect to dissociation will increase. At temperatures below some critical value, the lifetime of the H-bonded complex increases such that eventually every time such a complex forms it reacts via tunneling to form products. Under these low temperature conditions the overall rate constant for the reaction is determined not by the tunneling rate through the barrier, but rather by the rate of the barrierless association reaction. It is this general kinetic mechanism, one that involves a weakly bound complex of the reactants before a barrier that provides the recipe to dramatically enhance the rate of reaction only at low temperature. The crossover temperature for the transition from "normal" Arrhenius behavior to this unusual low-temperature behavior is determined by the binding energy of the complex and the shape (barrier height and width) of the activation barrier.

If we extend these ideas to H atom reactions with neutral closed-shell molecules in solid pH_2 we find some interesting similarities and differences. First, since the reaction is occurring in the presence of a solvent, there will not necessarily be an entrance channel well. The relative magnitudes of the reactant−reactant, reactant−pH_2, and pH_2−pH_2 intermolecular forces can result in a barrier or a well. Second, the importance of zero-point effects will be magnified because of the large translational zero point energies of the pH_2 solvent molecules and the H atom reactant. Third, the diffusion coefficient of an H atom in solid pH_2 is expected to be approximately independent of temperature[16] (quantum diffusion) below 4 K. Thus, if formation of the prereactive complex is stabilized, as the temperature is lowered, the association rate for complex formation remains constant but the dissociation rate rapidly decreases. This combination leads to the perfect storm by which tunneling reactions can only occur below some threshold temperature. In this case, the reaction rate gets accelerated to approach the diffusion limit at low temperature, and even tunneling reactions with very large barriers may become the dominant reaction. However, if the approach of the H atom to the coreactant is instead slightly uphill in energy (the prereactive complex is destabilized), then as the temperature is lowered the H atom has less thermal energy available to displace a pH_2 in the first solvation shell around the reactant molecule and the reaction rate constant should decrease. For small van der Waals barriers in the entrance channel (solvation barriers), we would expect the reaction to display Arrhenius type behavior where the added thermal energy helps to surmount this small barrier.

The proposed two-step kinetic mechanism presented in eqs 6 and 7 is therefore capable of explaining the inverse temperature effect measured in these studies. In the discussion so far we have assumed the H atom quantum diffusion rate is essentially constant over the temperature range from 1.7 to 4.3 K. Under this assumption, formation of a prereactive complex can help rationalize the inverse effect of temperature on the reaction rate. However, detailed measurements of the H atom quantum diffusion rate have not been performed in chemically doped pH_2 solids specifically under our low temperature reaction conditions. It could be the anomalous temperature dependence to the H + FA reaction stems not from the proposed low temperature formation of an encounter complex, but rather from qualitatively different quantum diffusion regimes that may exist over this small temperature range. For example, the diffusion coefficient of muonium in KCl and NaCl is known to increase by 3 orders of magnitude over the temperature range from 50 to 5 K as two-phonon processes increasingly play a dominant role in the low temperature quantum diffusion of muonium.[57] If a similar increase in the diffusion coefficient also occurs for H atom quantum diffusion in solid pH_2 then an alternative explanation of the inverse temperature effect could be related to the details of H atom quantum diffusion. It is known H atom quantum diffusion depends sensitively on the amounts of vacancies, oH_2, and crystal defects,[15] and thus it would be helpful to perform measurements on D_H under our experimental conditions that do not rely on detecting the reaction products.

Additionally it is not clear if structural changes in the FA solvation shell play a role in the observed inverse temperature dependence to the reaction kinetics. We speculate the reason the HOCO signal decays after photolysis at high temperature ($T > 2.7$ K) is due to the H + HOCO barrierless reaction that can occur at all temperatures, but is most pronounced at high temperature for some reason. It would be extremely helpful therefore if an IR absorption could be assigned to the H···FA encounter complex. We present data here that suggest the low energy wing of the FA ν_2 absorption may provide spectral signatures of the H−FA encounter complex. We observe a transient increase in the intensity of features observed in this region of the ν_2 absorption right after low temperature photolysis, but we also measure a strong reversible temperature dependence to these peaks that likely is due to changes in the structure of the $FA(oH_2)_n$ cluster. More definitive structural studies would require measuring the temperature dependence of the ν_2 absorption under comparable FA concentrations in the absence of H atoms. Finally, the role (if any) of oH_2 in the observed kinetics has not yet been explored either. Growth and destruction of oH_2 dimers[58,59] and large $CH_3F(oH_2)_n$ clusters[46,60] have been demonstrated previously over this same temperature range; at low temperature the clusters grow and at high temperature they decay. As documented here the majority of FA reagents exist as $FA(oH_2)_n$ clusters ($n \geq 1$), not as isolated FA reactants. In addition to changes in

dx.doi.org/10.1021/jp502470j | J. Phys. Chem. A XXXX, XXX, XXX−XXX

$FA(oH_2)_n$ cluster distributions and structures with temperature, diffusion of an H atom to an $FA(oH_2)_n$ cluster could result in NSC and release of significant amounts of H_2 rotational energy that could help trigger the reaction.

5. SUMMARY

We present FTIR spectroscopic measurements of the kinetics of low temperature tunneling reactions of H atoms with HCOOH and CO in solid pH_2. The reactions are initiated by generating H atoms within the pH_2 sample using the 193 nm in situ photolysis of HCOOH, and the reaction kinetics are measured after the photolysis is stopped. The concentration of HCOOH, CO, CO_2, HOCO, HCO and pH_2O can all be followed simultaneously for up to 10 h using FTIR spectroscopy. In six separate low-temperature experiments conducted on as-deposited samples at approximately 1.9 K, we measure first-order growth in the HOCO concentration with an average rate constant of $k = 4.9(7) \times 10^{-3}$ min^{-1}. We speculate the measured rate constant represents the association rate of the H···FA encounter complex that is directly related to the H atom quantum diffusion coefficient. However, as we also point out, the measured kinetics traces alone do not allow us to unambiguously identify the kinetics as being better described by the diffusion limited or slow reaction limiting cases. This points out the need for more experimental studies on H atom quantum diffusion under the low-temperature, chemically doped experimental conditions studied in this work and for theoretical studies of the energy landscapes in the entrance channel to reaction that include pH_2 solvation and zero-point energy contributions.

The most important finding of this study is the reaction kinetics for the H + FA reaction is qualitatively different at 4.3 and 1.9 K. We show that a two-step kinetic model that involves formation of the H−FA prereactive complex is consistent with the observed inverse temperature dependence; the slow tunneling reaction is only possible when the H−FA encounter complex is stabilized at low temperature. The fact that HOCO was not observed in similar reaction studies[21] conducted at 31 K in Kr matrices adds qualitative support for this interpretation. We have already published preliminary measurements[32] on the H + N_2O reaction in solid pH_2 that show a similar temperature dependence and therefore suggests this kinetic behavior may be general for H atom reactions with closed-shell molecules that have significant reaction barriers. These results could have large implications for understanding H atom reactions at extreme low temperatures, especially if H atom reactions in other surface or condensed phase systems display similar temperature dependencies. The diffusion rate of H atoms in solid pH_2 is anomalously high at low temperature due to the special properties of the diffusion mechanism; however, as this work shows, the low-temperature H atom chemistry may depend on the stabilities of weakly bound prereactive complexes and not on the relative rate constants for different tunneling reaction pathways.

■ ASSOCIATED CONTENT

Supporting Information

Table of the integrated absorption coefficients used to determine concentrations, FTIR spectra for double doping experiments used to assign FA−CO and H_2O−CO cluster peaks, expanded views of the ν_1 and ν_2 absorption features for HCO recorded at 1.65 and 4.36 K, table of the peak positions for *trans*-HOCO isolated in solid pH_2, window pane spectrum showing all the features assigned to *trans*-HOCO, expanded views of the ν_1 and ν_2 absorption features for *trans*-HOCO recorded at 1.65 and 4.36 K, tables of the kinetic parameters extracted from least-squares fits of the kinetic data to eq 3 and 4, representative fits of a sum of Lorentzian peaks to the FA $2\nu_3$ line shape, table of kinetic parameters for the growth/decay of $FA(oH_2)_n$ clusters for the experiment in Figure 4, spectrum of the FA ν_2 absorption showing the integration range used to determine the partial FA concentration. This material is available free of charge via the Internet at http://pubs.acs.org.

■ AUTHOR INFORMATION

Corresponding Author

*Mailing address: Department of Chemistry, University of Wyoming, Laramie, WY, 82071. Phone: 307-766-2775; e-mail: danderso@uwyo.edu.

Present Address

†Department of Environmental Quality, 122 W. 25th Street, Cheyenne, WY 82002.

Notes

The authors declare no competing financial interest.

■ ACKNOWLEDGMENTS

We thank Kylie A. Kufeld for contributing to some of the experiments presented in this work during her visit in 2011 from March to June while she was an undergraduate chemistry major at Dartmouth College. We also like to thank Prof. Robert J. Hinde for many valuable discussions about the implications of the proposed two-step reaction mechanism in solid pH_2. The authors thank the National Science Foundation for its generous support through Grant CHE 08-48330.

■ REFERENCES

(1) Benderskii, V. A.; Goldanskii, V. I.; Makarov, D. E. Quantum Dynamics in Low-Temperature Chemistry. *Phys. Rep.* **1993**, *233*, 195−339.

(2) Skouteris, D.; Manolopoulos, D. E.; Bian, W.; Werner, H.-J.; Lai, L.-H.; Liu, K. van der Waals Interactions in the Cl + HD Reaction. *Science* **1999**, *286*, 1713.

(3) Shannon, R. J.; Taylor, S.; Goddard, A.; Blitz, M. A.; Heard, D. E. Observation of a Large Negative Temperature Dependence for Rate Coefficients of Reactions of OH with Oxygenated Volatile Organic Compounds Studied at 86−112 K. *Phys. Chem. Chem. Phys.* **2010**, *12*, 13511−13514.

(4) Czako, G.; Bowman, J. M. Dynamics of the Reaction of Methane with Chlorine Atom on an Accurate Potential Energy Surface. *Science* **2011**, *334*, 343−346.

(5) Marx, D.; Tuckerman, M. E.; Hutter, J.; Parrinello, M. The Nature of the Hydrated Excess Proton in Water. *Nature* **1999**, *397*, 601−604.

(6) Miyazaki, T.; Lee, K.-P.; Fueki, K.; Takeuchi, A. Temperature Effect on the Decay of H (D) Atoms in the Radiolysis of Solid H_2, D_2, and HD at 4.2 and 1.9 K. Evidence for Tunneling Migration. *J. Phys. Chem.* **1984**, *88*, 4959−4963.

(7) Kumada, T.; Mori, S.; Nagasaka, T.; Kumagai, J.; Miyazaki, T. Resonance Effect on the Tunneling Reaction: H + H_2 → H_2 + H in Solid Hydrogen. *J. Low Temp. Phys.* **2001**, *122*, 265−277.

(8) Kumada, T. Experimental Determination of the Mechanism of the Tunneling Diffusion of H Atoms in Solid Hydrogen: Physical Exchange Versus Chemical Reaction. *Phys. Rev. B* **2003**, *68*, 052301.

(9) Takayanagi, T.; Masaki, N. M.; Nakamura, K.; Okamoto, M.; Sato, S.; Schatz, G. C. The Rate Constants for the H+H_2 Reaction and its Isotopic Analogs at Low Temperatures: Wigner Threshold Law Behavior. *J. Chem. Phys.* **1987**, *86*, 6133.

(10) Hancock, G. C.; Mead, C. A.; Truhlar, D. G.; Varandas, A. J. C. Reaction Rates of $H(H_2)$, $D(H_2)$, and $H(D_2)$ van der Waals Molecules and the Threshold Behavior of the Bimolecular Gas Phase Rate Coefficient. *J. Chem. Phys.* **1989**, *91*, 3492.
(11) Ivliev, A. V.; Katunin, A. Y.; Lukashevich, I. I.; Sklyarevskii, V. V.; Suraev, V. V.; Filippov, N. I.; Shevtsov, V. A. Temperature-Dependence of Quantum Diffusion of H-atoms in Solid H_2 in the Temperaure Range 1.35 to 4.2 K. *JETP Lett.* **1982**, *36*, 472.
(12) Iskovskikh, A. S.; Katunin, A. Y.; Lukashevich, I. I.; Sklyarevskii, V. V.; Suraev, V. V.; Filippov, N. I.; Shevtsov, V. A. Recombination and Spin Relaxation of Hydrogen and Deuterium Atoms in Molecular-Crystals. *Sov. Phys. JETP* **1986**, *91*, 1832−1848.
(13) Kumada, T.; Kitagawa, N.; Noda, T.; Kumagai, J.; Aratono, Y.; Miyazaki, T. An ENDOR Spectrum of H Atoms in Solid H_2. *Chem. Phys. Lett.* **1998**, *288*, 755−759.
(14) Miyazaki, T.; Mori, S.; Nagasaka, T.; Kumagai, J.; Aratono, Y.; Kumada, T. Decay Dynamics of H Atoms in Solid Hydrogen at 4.2 K. Controlling Factor of Tunneling Reaction H + *para*-H_2 → *para*-H_2 + H. *J. Phys. Chem. A* **2000**, *104*, 9403−9407.
(15) Miyazaki, T.; Kumagai, J.; Kumada, T. Controlling Factors of Tunneling Reactions in Solid Hydrogen at Very Low Temperature. *Radiat. Phys. Chem.* **2001**, *60*, 381.
(16) Kumada, T.; Sakakibara, M.; Nagasaka, T.; Fukuta, H.; Kumagai, J. Absence of Recombination of Neighboring H Atoms in Highly Purified Solid Parahydrogen: Electron Spin Resonance, Electron-Nuclear Double Resonance, and Electron Spin Echo Studies. *J. Chem. Phys.* **2002**, *116*, 1109−1119.
(17) Kumada, T.; Shimizu, Y.; Ushida, T.; Kumagai, J. H Atom, e^-, and H_6^+ Ions Produced in Irradiated Solid Hydrogens: An Electron Spin Resonance Study. *Radiat. Phys. Chem.* **2008**, *77*, 1318−1322.
(18) Fushitani, M.; Momose, T. A Study on Diffusion of H atoms in Solid Parahydrogen. *Low Temp. Phys.* **2003**, *29*, 740−743.
(19) Andrews, L.; Wang, X. Infrared Spectra of H_2 Molecules Near H atoms Trapped in Solid H_2. *J. Phys. Chem. A* **2004**, *108*, 3879−3883.
(20) Andrews, L.; Wang, X. A Discharge Investigation of Hydrogen and Deuterium Atom Formation, and Parahydrogen and Orthodeuterium Reconversion. *J. Chem. Phys.* **2004**, *121*, 4724−4729.
(21) Cao, Q.; Berski, S.; Latajka, Z.; Räsänen, M.; Khriachtchev, L. Reaction of Atomic Hydrogen with Formic Acid. *Phys. Chem. Chem. Phys.* **2014**, *16*, 5993−6001.
(22) Su, H.; He, Y.; Kong, F.; Fang, W.; Liu, R. Photodissociation of Formic Acid. *J. Chem. Phys.* **2000**, *113*, 1891−1897.
(23) Shin, S. K.; Han, E. J.; Kim, H. L. Photodissociation Dynamics of Formic Acid at 193 nm. *J. Photochem. Photobiol., A* **1998**, *118*, 71−74.
(24) He, H.-Y.; Fang, W.-H. A CASSCF/MR-CI Study Toward the Understanding of Wavelength-Dependent and Geometrically Memorized Photodissociation of Formic Acid. *J. Am. Chem. Soc.* **2003**, *125*, 16139−16147.
(25) Kurosaki, Y.; Yokoyama, K.; Teranishi, Y. Direct Ab Initio Molecular Dynamics Study of the Two Photodissociation Channels of Formic Acid. *Chem. Phys.* **2005**, *308*, 325−334.
(26) Huang, C.; Zhang, C.; Yang, X. State-Selected Imaging Studies of Formic Acid Photodissociation Dynamics. *J. Chem. Phys.* **2010**, *132*, 154306.
(27) Martínez-Núnez, E.; Vázquez, S. A.; Borges, I., Jr.; Rocha, A. B.; Estévez, C. M.; Castillo, J. F.; Aoiz, F. J. On the Conformational Memory in the Photodissociation of Formic Acid. *J. Phys. Chem. A* **2005**, *109*, 2836−2839.
(28) Martínez-Núnez, E.; Vázquez, S. A.; Granucci, G.; Persico, M.; Estevez, C. M. Photodissociation of Formic Acid: A Trajectory Surface Hopping Study. *Chem. Phys. Lett.* **2005**, *412*, 35−40.
(29) Wonderly, W. R.; Anderson, D. T. Transient HDO Rovibrational Satellite Peaks in Solid Parahydrogen: Evidence of Hydrogen Atoms or Vacancies? *Low Temp. Phys.* **2012**, *38*, 853−859.
(30) Kufeld, K. A.; Wonderly, W. R.; Paulson, L. O.; Kettwich, S. C.; Anderson, D. T. Transient H_2O Infrared Satellite Peaks Produced in UV Irradiated Formic Acid Doped Solid Parahydrogen. *J. Phys. Chem. Lett.* **2012**, *3*, 342−347.
(31) Krasnoperov, L. N.; Chesnokov, E. N.; Stark, H.; Ravishankara, A. R. Elementary Reactions of Formyl (HCO) Radical Studied by Laser Photolysis — Transient Absorption Spectroscopy. *Proc. Combust. Inst.* **2005**, *30*, 935−943.
(32) Mutunga, F. M.; Follett, S. E.; Anderson, D. T. Communication: H-Atom Reactivity as a Function of Temperature in Solid Parahydrogen: The H+N_2O Reaction. *J. Chem. Phys.* **2013**, *139*, 151104.
(33) Wonderly, W. R.; Anderson, D. T. Reactions of Atomic Hydrogen with Formic Acid and Carbon Monoxide in Solid Parahydrogen II: Deuterated Reaction Studies. *J. Phys. Chem. A* **2014**, DOI: 10.1021/jp502469p.
(34) Paulson, L. O.; Anderson, D. T. High-Resolution Vibrational Spectroscopy of *trans*-Formic Acid in Solid Parahydrogen. *J. Phys. Chem. A* **2009**, *113*, 1770−1778.
(35) Fajardo, M. E.; Tam, S. Rapid Vapor Deposition of Millimeters Thick Optically Transparent Parahydrogen Solids for Matrix Isolation Spectroscopy. *J. Chem. Phys.* **1998**, *108*, 4237−4241.
(36) Tam, S.; Fajardo, M. E. Ortho/Para Hydrogen Converter for Rapid Depostion Matrix Isolation Spectroscopy. *Rev. Sci. Instrum.* **1999**, *70*, 1926−1932.
(37) Fajardo, M. E. Matrix Isolation Spectroscopy in Solid Parahydrogen: A Primer. In *Physics and Chemistry at Low Temperatures*; Khriachtchev, L., Ed.; Pan Stanford Publishing: Singapore, 2011; pp 167−202.
(38) Silvera, I. F. The Solid Molecular Hydrogens in the Condensed Phase: Fundamentals and Static Properties. *Rev. Mod. Phys.* **1980**, *52*, 393−452.
(39) Paulson, L. O.; Anderson, D. T. Infrared Spectroscopy of the Amide I Mode of N-Methylacetamide in Solid Hydrogen at 2−4 K. *J. Phys. Chem. B* **2011**, *115*, 13659−13667.
(40) Fajardo, M. E.; Lindsay, C. M.; Momose, T. Crystal Field Theory Analysis of Rovibrational Spectra of Carbon Monoxide Monomers Isolated in Solid Parahydrogen. *J. Chem. Phys.* **2009**, *130*, 244508.
(41) Tam, S.; Fajardo, M. E. Observation of the High-Resolution Infrared Absorption Spectrum of CO_2 Molecules Isolated in Solid Parahydrogen. *Low Temp. Phys.* **2000**, *26*, 653−660.
(42) Lundell, J.; Räsänen, M. The 193 nm Induced Photo-decompostiion of HCOOH in Rare Gas Matrices: The H_2O−CO 1:1 Complex. *J. Phys. Chem.* **1995**, *99*, 14301−14308.
(43) Lundell, J.; Räsänen, M. Photochemistry of Formic Acid in Rare Gas Matrices: Double-Doping Experiments on the 193 nm Induced Photodecomposition. *J. Mol. Struct.* **1997**, *436*−*437*, 349−358.
(44) Olbert-Majkut, A.; Ahokas, J.; Lundell, J.; Pettersson, M. Photolysis of HCOOH Monomer and Dimer in Solid Argon: Raman Characterization of In Situ Formed Molecular Complexes. *Phys. Chem. Chem. Phys.* **2010**, *12*, 7138−7147.
(45) Momose, T.; Fushitani, M.; Hoshina, H. Chemical Reactions in Quantum Crystals. *Int. Rev. Phys. Chem.* **2005**, *24*, 533.
(46) Yoshioka, K.; Raston, P. L.; Anderson, D. T. IR Spectroscopy of Chemically Doped Solid pH_2. *Int. Rev. Phys. Chem.* **2006**, *25*, 469−496.
(47) Ruzi, M.; Anderson, D. T. Photodissociation of *N*-Methylformamide Isolated in Solid Parahydrogen. *J. Chem. Phys.* **2012**, *137*, 194313.1−194313.11.
(48) Raston, P. L.; Anderson, D. T. Infrared-Induced Reaction of Cl Atoms Trapped in Solid Parahydrogen. *Phys. Chem. Chem. Phys.* **2006**, *8*, 3124−3129.
(49) Lossack, A. M.; Bartels, D. M.; Roduner, E. Rate Constants and Kinetic Isotope Effects in Hydrogen Abstractions by H from Formic Acid. *Res. Chem. Intermed.* **2001**, *27*, 475−483.
(50) Hou, H.; Wang, B. Mechanistic and Kinetic Study of the O + CH_2OH Reaction. *J. Phys. Chem. A* **2005**, *109*, 4796−4803.
(51) Carroll, F. A.: *Perspectives on Structure and Mechanism in Organic Chemistry*; Brooks/Cole Publishing Company: New York, 1998.
(52) Marshall, P.; Glarborg, P. Ab Initio and Kinetic Modeling Studies of Formic Acid Oxidation. *Proc. Combust. Inst.* **2014**, DOI: 10.1016/j.proci.2014.05.091.

(53) Wang, H. Y.; Eyre, J. A.; Dorfman, L. M. Activation Energy for the Gas Phase Reaction of Hydrogen Atoms with Carbon Monoxide. *J. Chem. Phys.* **1973**, *59*, 5199−5200.
(54) Song, L.; van der Avoid, A.; Groenenboom, G. C. Three-Dimensional Ab Initio Potential Energy Surface for H−CO($\tilde{X}^2A'$). *J. Phys. Chem. A* **2013**, *117*, 7571−7579.
(55) Steinfeld, J. I.; Francisco, J. S.; Hase, W. L.: *Chemical Kinetics and Dynamics*; 2nd ed.; Prentice Hall: Upper Saddle River, NJ, 1999.
(56) Fernandez-Ramos, A.; Miller, J. A.; Klippenstein, S. J.; Truhlar, D. G. Modeling the Kinetics of Bimolecular Reactions. *Chem. Rev.* **2006**, *106*, 4518−4584.
(57) Kagan, Y.; Prokofev, N. V. Quantum Diffusion of Muonium in KCl and NaCl. *Phys. Lett. A* **1990**, *150*, 320−326.
(58) Boggs, S. A.; Welsh, H. L. An Infrared Spectroscopic Study of Quantum Diffusion in Solid Hydrogen. *Can. J. Phys.* **1973**, *51*, 1910−1914.
(59) Roffey, B. J.; Boggs, S. A.; Welsh, H. L. Infrared Studies of Quantum Diffusion in Solid Hydrogen. *Can. J. Phys.* **1974**, *52*, 2451−2453.
(60) Yoshioka, K.; Anderson, D. T. Preferential Solvation of CH_3F by ortho-H_2 in Cryogenic Solid Hydrogen. *J. Mol. Struct.* **2006**, *786*, 123−129.